NANOMATERIALS AND THE ENVIRONMENT
Research Article • DOI: 10.2478/nanome-2013-0001 • NANOME • 2013 • 1–8

VERSITA

TiO_2-doped resorcinol–formaldehyde (RF) polymer and carbon gels with photocatalytic activity

Abstract
Resorcinol-formaldehyde (RF) polymer gels offer a relatively easy and versatile route for incorporating metals into a carbon aerogel matrix. The hybrid materials thus obtained are ideal candidates for applications involving enhanced adsorption or catalysis. This paper presents a detailed study of Ti-doped RF and carbon aerogels. The metal was introduced into the system at three different stages of the preparation process: during polymerization, by impregnation of the RF gel, or by impregnation of the carbon gel. The structure and morphology of the samples are compared using low temperature N_2 adsorption, SEM, and small and wide angle X-Ray scattering (SAXS/WAXS) methods. The TiO_2-doped carbon aerogels display photocatalytic activity in breaking down aromatic compounds.

Keywords
Carbon aerogel • Hybrid material • Adsorption • SAXS/WAXS • Titanium doping • Photocatalyst

Orsolya Czakkel[1,2*], Erik Geissler[3], Imre M. Szilágyi[4], Krisztina László[1]

[1]Department of Physical Chemistry and Materials Science, Budapest University of Technology and Economics, H-1521 Budapest, Hungary

[2]Present address: Institute Laue-Langevin, BP 156, 38042 Grenoble France

[3]Laboratoire Interdisciplinaire de Physique CNRS UMR 5588, Université J. Fourier de Grenoble, BP 87, 38402 St Martin d'Hères Cedex, France

[4]Research Group of Technical Analytical Chemistry of the Hungarian Academy of Sciences, Department of Inorganic and Analytical Chemistry, Budapest University of Technology and Economics, H-1111 Budapest, Szt. Gellért tér 4., Hungary

Received 02 October 2012
Accepted 31 January 2013

1. Introduction

Mesoporous carbon gels are prepared by carbonization of polymers, most often resorcinol-formaldehyde (RF) gels. If the adsorption or catalytic potential of these materials is to be enhanced, consideration must be given to incorporating metal ions. Owing to their complex synthesis route RF gels have the advantage that metal ions can be introduced relatively easily, either in the sol–gel process or by impregnation of the network. Several studies have been made on doped carbon gels with the aim of incorporating the metal during the polymerization reaction. If the conventional catalyst, sodium carbonate, is replaced by different metal salts at the outset of the preparation process, the metal salt becomes trapped within the gel structure and the metal ions may be chelated by the functional groups of the polymer matrix. They can also affect the morphology and the pore texture of the organic aerogel [1]. A study of the formation of carbon aerogels doped with Fe^{2+}, Co^{2+}, Ni^{2+} and Cu^{2+} concluded that the morphology and textural characteristics of the network are determined mainly by the pH, which is defined by the chemical character of the metal ion [1,2]. Pt^{2+}, Pd^{2+}, Ag^{+} and Ti^{4+} were also found to exert a strong influence on the aerogel architecture [3-5]. By contrast, Sanchez-Polo *et al*. found that addition of a transition metal (Ag^{+}, Co^{2+}, Mn^{2+}, Ti^{4+}) to the reaction mixture does not markedly influence the textural and chemical properties of the RF aerogel [6]. When sodium carbonate is replaced by another metal salt with basic character (e.g., K^{+}, Mg^{2+}, Zr^{4+}), carbon with highly dispersed metal oxide particles can be produced. In this way, the porous texture of the carbonaceous component can be combined with the basic properties of the oxides. [7]. In some cases (e.g., Pd^{2+}, Fe^{2+}, Co^{2+}, Cu^{2+} or Ni^{2+} salts) an additional complexing agent is needed to keep the metal in solution. Texture analysis showed that the complexant modifies the microporous texture of the samples and that the presence of metal salt affects the mesopore range. Furthermore, Fu *et al*. [8] found that during the carbonization process, metal loaded samples may become partially graphitized. Czakkel *et al*. [9,10] showed that the presence of Cu^{2+} during the polymerization changes dramatically the reaction between resorcinol and formaldehyde, and although Cu cannot be built into the structure in this way, the resulting RF and carbon gel has outstanding pore properties. By contrast, Cu can be introduced into the matrix by post-impregnation of the RF or carbon gels with a Cu^{2+} salt solution, but this reduces the porosity. Recent work on Mo-containing RF gels also showed that molybdenum modifies the synthesis reaction, forming glass-like granules instead of network monoliths [11].

In our study titanium is introduced at three different stages of the preparation process. Under the synthesis conditions, titanium dioxide is formed, which holds promise as an efficient photocatalyst [12]. A combination of different characterization techniques (scanning electron microscopy, SEM; low temperature N_2 adsorption/desorption, small/wide angle X-Ray scattering measurements, SAXS/WAXS) was employed to determine structural differences among the samples. This paper reports the effect of Ti^{4+} on the morphology of the RF and carbon gels and compares the catalytic potential of the doped carbon materials.

* *E-mail: czakkelo@ill.fr*

2. Experimental

2.1. Materials

2.1.1. Sample preparation

The detailed preparation process of the monolithic RF hydrogels is described elsewhere [13]. Briefly, a 5% (wt/v) aqueous solution of resorcinol (R), formaldehyde (F) and sodium carbonate (C) was prepared with molar ratios R/F=0.5 and R/C=50. The initial pH of the solution was adjusted to pH 6.0 with dilute HNO_3. The RF sol was kept at 85°C for a week to complete the gelation.

Ti-doped RF gels were prepared according to the method of Maldonado-Hódar *et al.* [14]. After dissolving the resorcinol and the formaldehyde in distilled water, the solution was heated to 60°C. The allotted amount of titanium tetraisopropoxide (TTIP) was added dropwise, with continuous stirring of the solution. The mixture was then aged for 4 h at 60°C. This reaction yielded a precipitate, rather than a macroscopic network monolith. The molar ratios R/F and R/W were the same as for the basic RF gel, while the molar ratio of R and the TTIP was 1. After filtration the precipitate was washed with acetone for three days to prepare for the drying procedure.

Ti-impregnated RF and carbon gels were prepared by soaking either the dried RF aerogels or the carbon gels for 24 h at room temperature in 0.04 M TTIP solution. The solvent used was acetone and 75 ml solution was used for 1 g gel.

2.1.2. Drying

The opaque brown-orange hydrogels were placed in three times their own volume of acetone (extra pure) for 3 days, and the solvent renewed every day. For drying, supercritical CO_2 extraction was performed with a continuous solvent flow of 1.2 ml/min. The applied pressure and temperature were 100 bar and 43°C, respectively. After washing for 70 minutes, the pressure in the cell was slowly reduced to obtain the RF aerogels. Details of the experimental setup are given elsewhere [15].

2.1.3. Carbonization

Carbonization was performed in a rotary quartz reactor at 900°C for 1 h in a 25 ml/min flow of high purity nitrogen.

2.2. Methods

2.2.1. Scanning Electron Microscopy/Energy-dispersive X-ray spectroscopy (SEM/EDX)

Surface morphological investigations were made on a JEOL 5500 (JEOL, Japan) electron microscope in high vacuum mode with a secondary electron detector. The accelerating voltage was 20 kV and the working distance varied between 5 and 27 mm. Samples were fastened to a copper sample holder by adhesive carbon tape. The polymer samples were coated with Au/Pd to prevent charging. Elemental analyses were performed on the metal-doped RF and carbon gels by the Ka lines of the elements, using the same apparatus in high vacuum mode. The applied magnification was 5000x, and the average metal concentrations were calculated from at least six different measurements.

2.2.2. Low temperature N_2 adsorption/desorption,

Nitrogen adsorption/desorption isotherms were measured at –196°C with an Autosorb-1 (Quantachrome, USA) computer controlled volumetric gas adsorption apparatus. Prior to the measurements, the samples were evacuated at 20°C for 24 h at $p < 3 \cdot 10^{-4}$ mbar. To quantify differences in the structure of the samples several parameters were deduced from the adsorption/desorption isotherms. Gas adsorption gives information on the pore diameter d only in the micropore (d < 20 Å) and part of the mesopore (20 Å < d < 300 Å) range. The upper limit of these calculations is set by the exponential nature of the relationship $d = f(p/p_0)$ [16]. In certain samples, owing to capillary condensation, the uncertainty in the estimate of the total pore volume (V_{TOT}) obtained from the region $p/p_0 \rightarrow 1$ of the isotherms can be very high. For this reason, the pore volume ($V_{0.94}$) was derived from the amount of vapour adsorbed at relative pressure 0.94, assuming that the pores are then filled with liquid adsorbate; this corresponds to pores with d < 305 Å. Thus, $V_{meso} = V_{0.94} - W_0$ is the volume of the mesopores of diameter smaller than 305 Å, and $V_{macro} = V_{TOT} - V_{0.94}$ is the volume of all the pores detected by nitrogen adsorption that are larger than d = 305 Å. The apparent surface area (S_{BET}) was calculated using the Brunauer–Emmett–Teller (BET) model [17]. The micropore volume (W_0) and micropore width (w) were derived by the Dubinin–Radushkevich (DR) method, and the b parameter was 0.391. The pore size distribution (PSD) in the mesopore range was determined from the adsorption branch by the BJH model. The DFT method for the micropore analysis was inapplicable in our case due to the lack of kernel for the hybrid metal-carbon systems. The calculations were performed with the Quantachrome software (ASiQwin 2.01).

2.2.3. Small/wide angle X-Ray scattering measurements, SAXS/WAXS

SAXS/WAXS measurements of the dry and carbonized samples were made on the BM2 small angle camera in the European Synchrotron Radiation Facility (ESRF), Grenoble, France. The transfer wave vector range explored was $0.0019 < q < 5.7$ Å^{-1}, where

$$q = 4\pi \sin(\theta/2)/\lambda \quad (1)$$

θ being the scattering angle and λ the wavelength of the incident radiation. An indirect illumination CCD detector (Princeton Instruments) with effective pixel size 50 mm was used. Intensity curves, $I(q)$, obtained by azimuthal averaging, were corrected for grid distortion, dark current, sample transmission and also for background scattering. The powdered samples were placed in glass capillary tubes of diameter 1.5 mm. Intensities were normalized with respect to a standard sample (lupolen), assuming an effective sample thickness of 1 mm to account approximately for the filling factor of the powder. The resulting

error in the stated absolute values of the intensity is expected to be no greater than 25%. The size of the elementary scattering units was calculated on the assumption that the structure is composed of spherical beads. Details of the calculation are given elsewhere [9].

2.2.4. Photocatalytic activity test

Photocatalytic activity of the Ti-doped carbons was probed by methylene blue and phenol decomposition tests [18,19]. 5 ml methylene blue (MEB) solution (20 mg/l) was added to 5 ml 0.1 wt/v% aqueous suspension of the carbon gels. The measurements were performed in a Solarbox containing six lamps ($\lambda \geq 310$ nm; 6x25 W). The distance between the sample and the light source was 10 cm. Prior to the UV irradiation a delay time of 10 minutes was observed to allow for adsorption. The suspension was stirred continuously during the 12-minute test, and the concentration of MEB was determined every 2 minutes by UV spectrophotometry.

Decomposition of phenol was investigated in a cylindrical double walled photoreactor, with a mercury vapor lamp (350 W) as light source. The sample suspension (0.5 mM phenolic solution + 0.05 wt/v% carbon aerogel suspension) was continuously stirred, and also cooled to offset heating by the lamp (the temperature rose from the initial 20°C to 35°C). Continuous airflow was maintained throughout the 120 min irradiation, because the presence of O_2 is necessary for the photodegradation process. The change in phenol concentration of the suspension was measured every 20 minutes by a liquid chromatography instrument equipped with a UV detector. In both cases, commercial *Degussa P25 TiO_2* (49 m^2/g) was used as a reference.

3. Results and discussion

3.1. Polymer gels

To examine the effect of the method of metal doping, titanium was introduced at three different stages of the sol–gel process, by (1) addition to the precursor mixture, (2) impregnation of the dried polymer gels, and (3) impregnation of the carbon gel. The nomenclature of the samples is listed in Table 1.

Addition of TTIP to the aqueous reaction mixture of the resorcinol and formaldehyde promptly yields a thick, yellow precipitate. Unlike standard monolithic RF gels, after drying, the sample (*TiP*) is a powder, i.e., no Ti-containing monoliths were obtained by this method. SEM images in Figure 1 reveal that the inclusion of TTIP into all the systems results in a more compact structure than the dopant-free samples. In the *TiP* sample even the beads become indistinguishable at the SEM resolution employed.

The differences in the morphology are also reflected in the adsorption isotherms (Figure 2a). In both doped samples the nitrogen adsorption capacity is substantially reduced. The isotherm of *TiP*, like that of the undoped sample *P*, is of Type IIb [20]. Post-impregnation modifies the adsorption isotherms to Type IVa. The change in the nature of the hysteresis loop indicates a narrow mesopore size distribution, which is typical for compact spheroidal particles of fairly uniform size [16].

The parameters deduced from the adsorption isotherms are listed in Table 2. In all categories the pore volume is lowest for the *TiP* precipitate, in accordance with its compact structure. The incorporation of TTIP into the samples (independently of the method of introduction) reduces both micro- and mesoporosity (Figure 3a, Table 2).

SAXS/WAXS measurements offer a means of detecting differences in the morphology at submicrometre length scales. Post-impregnation of *P* using TTIP in acetone does not affect the structure at the larger end of the submicrometre scale, as reflected by the slopes of the SAXS responses in the region of $0.005\ Å^{-1} \leq q \leq 0.01\ Å^{-1}$ (Figure 4a). In the higher q-region of this aerogel the slope of –2.6 indicates volume scattering. This feature is qualitatively different from *P*, where the slope –3.6 corresponds to scattering from rough surfaces. Determination of the size of the elementary scattering units from the Iq^4 vs. q representation of the scattering signal could be made only for *P* and *PTi*. This showed that post-impregnation increases the size of the elementary beads from 71 Å, as in the undoped *P* sample, to 100 Å. The shape of the SAXS curve in sample *TiP*

Table 1. Nomenclature of the prepared RF and carbon gels.

Label	Description
P	Polymer aerogel, RF gel dried with supercritical CO_2 extraction
TiP	*P* synthesized in the presence of Ti
PTi	*P*, post-impregnated with Ti-solution
PC	*P*, carbonized
TiPC	*TiP*, carbonized
PTiC	*PTi*, carbonized
PCTi	*PC*, post-impregnated with Ti-solution

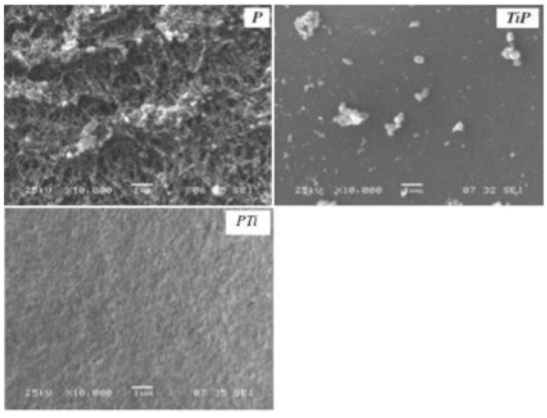

Figure 1. SEM images (x10000, scalebar = 1 μm) of the aerogels.

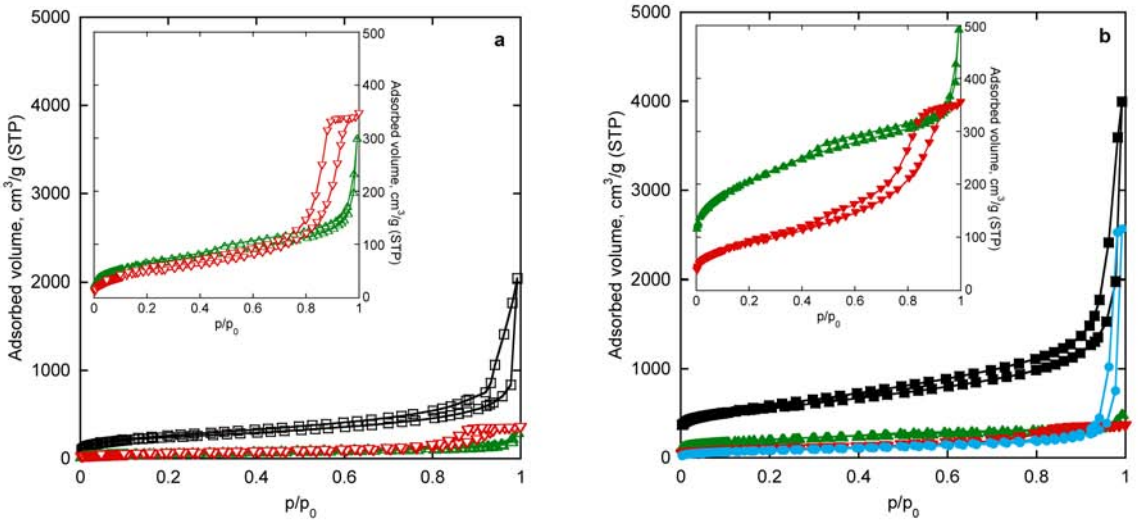

Figure 2. N_2 *adsorption/desorption isotherms of (a) P (□), TiP (△), PTi (▽) aerogels and (b) PC (■), TiPC (▲), PTiC (▼), PCTi (●) carbon gels.*

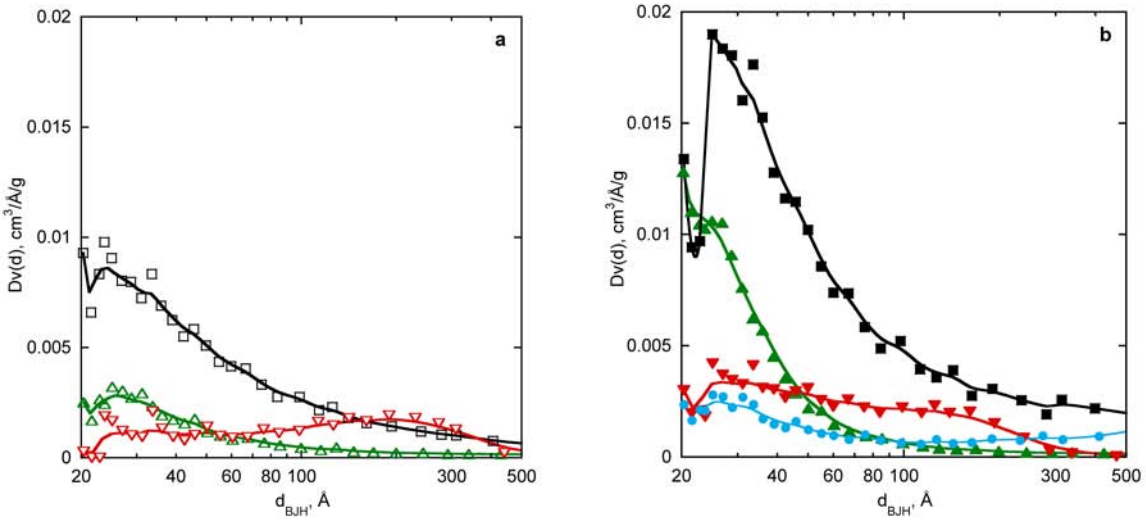

Figure 3. Pore size distribution of P (□), TiP (△), PTi (▽) aerogels and PC (■), TiPC (▲), PTiC (▼), PCTi (●) carbon gels calculated from the adsorption branch by the BJH method.

Table 2. Yield and morphology data from nitrogen adsorption measurements of P, PC, and the Ti-doped derivates.

Sample	*Ti content (%)**	*Yield* %	S_{BET} m²/g	*C*	V_{TOT} cm³/g	$V_{0.94}$ cm³/g	W_0 cm³/g	*slope*	V_{meso} cm³/g	V_{macro} cm³/g
P		-	846	168	3.16	0.87	0.27	–3.9	0.60	2.29
TiP		-	223	155	0.47	0.20	0.07	–3.6	0.13	0.27
PTi		-	164	140	0.52	0.33	0.04	–5.8	0.29	0.21
PC		38	1990	652	6.15	1.83	0.78	–2.5	1.05	4.32
TiPC	27 ±1.5	50	718	435	0.77	0.50	0.25	–2.2	0.25	0.27
PTiC	72 ±4.0	48	306	226	0.54	0.47	0.10	–3.9	0.37	0.07
PCTi	15 ±0.5	-	301	95	3.98	0.37	0.09	–5.4	0.28	3.61

**From EDX measurements. Yield: yield of the carbonization, S_{BET}: apparent surface area, C: interaction parameter in the net energy of adsorption, V_{TOT}: total pore volume at $p/p_0 \rightarrow 1$, $V_{0.94}$: pore volume derived from adsorbed volume at $p/p_0 = 0.94$, W_0: micropore volume from DR analysis, slope: slope of the DR plot ($\sim E^{-2}$, E: characteristic adsorption potential); $V_{meso} = V_{0.94} - W_0$, $V_{macro} = V_{TOT} - V_{0.94}$.*

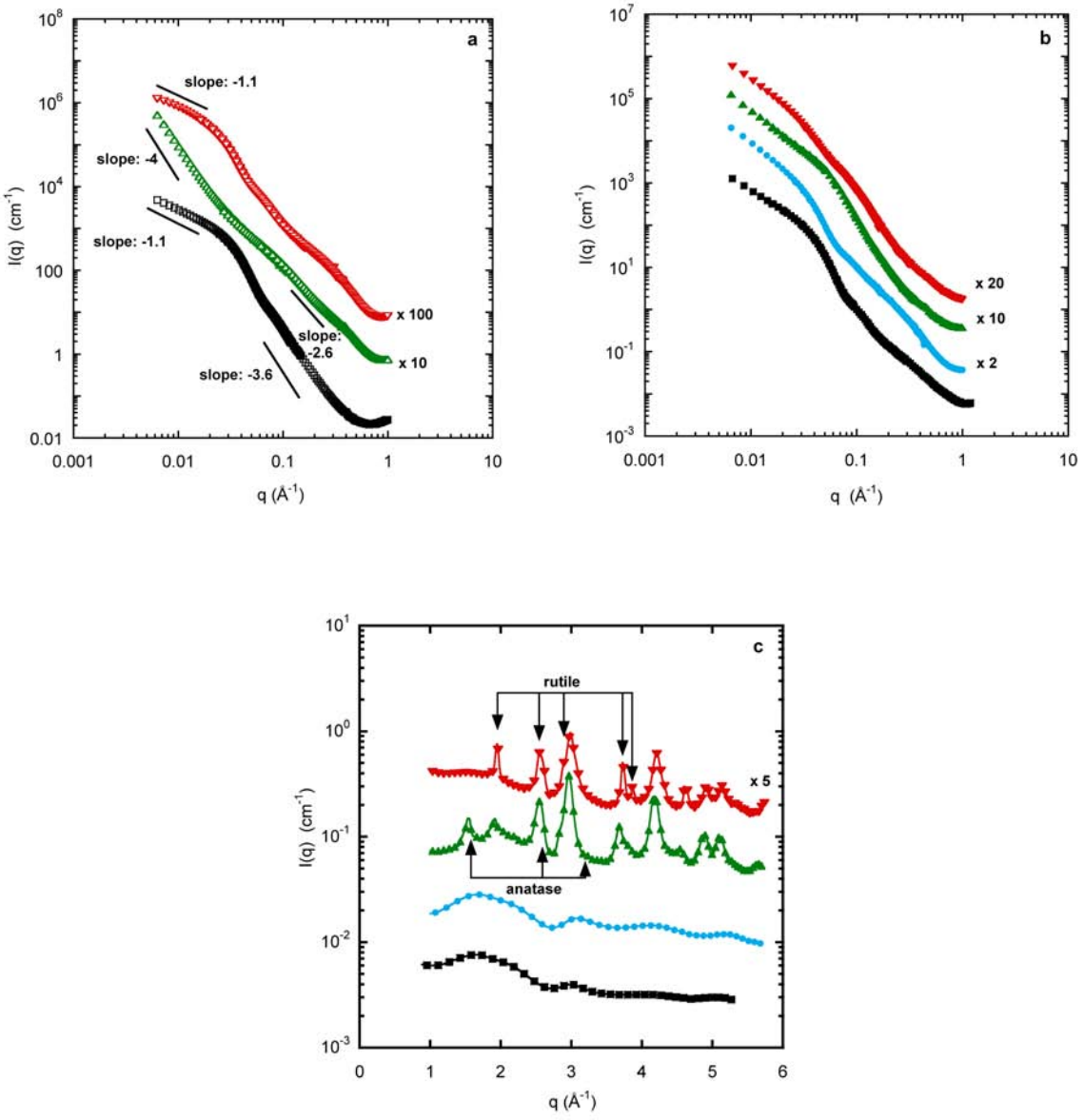

Figure 4. SAXS response of (a) P (□), TiP (△), PTi (▽) aerogels and (b) PC (■), TiPC (▲), PTiC (▼), PCTi (●) carbon gels. (c) WAXS signal of the carbon gels.

(power law slope of –4 in the lowest *q* region) is the signature of large aggregates of size greater than the resolution limit of the measurement (~1000 Å). In the higher *q*-range, which explores the interior of the aggregates, the slope decreases to –2.6, similar to that expected for a branched structure.

3.2. Titania doped carbon gels

Ti-doped carbon gels were obtained either by pyrolysis of the Ti-containing RF aerogel or by post-impregnation of the carbon aerogel. The SEM images in Figure 5 indicate that the loose structure of the doped polymer samples is conserved in the pyrolysis and even the relatively smooth surface of sample *TiP* becomes highly structured.

The carbonized *P*, *TiP* and *PTi* samples (*PC*, *TiPC*, *PTiC*, respectively) exhibit enhanced microporosity (Figure 2b, Table 2). The shape of the PSD curves resembles that of the parent polymers. Post impregnation has the same effect on *PC* as was observed with the polymer. The *C* parameter of the BET model and the slope of the DR plot (Table 2) reveal the differences in surface energy of the carbonized samples and also show that carbonization enhances the adsorption interactions. This is due in part to the increased microporosity.

The SAXS response curves of the carbonized Ti-doped samples exhibit only slight structural differences. The large-scale structure is basically identical in all the samples (Figure 4b), but the radius of the elementary beads, estimated from the Iq^4 vs. *q* representation, varies substantially (Table 3). As might be expected, carbonization reduces their size [9], while post-impregnation results in a slight increase. The heat treatment also modifies the titanium. The WAXS responses of *TiPC* and

PTiC (Figure 4c) exhibit Bragg reflections corresponding to TiO_2. The distinction between the different crystalline forms of TiO_2 [21] is, however, important, since their photocatalytic activity differs considerably. Rutile is the most commonly obtained form in sol - gel preparation processes. Although anatase has superior charge carrier properties (wider band gap, smaller electron effective mass, higher Fermi level etc.) [22], in ambient conditions, it is thermodynamically unstable [23] and undergoes a polymorphic transformation to rutile at high temperatures [24]. Several parameters, such as impurities, particle size or surface area, affect the thermodynamic equilibrium of the two forms. Moreno-Castilla et al. [5] found that in carbon aerogel/ titania composite materials the carbon matrix prevents sintering of titania nanoparticles and stabilizes the polymorphic anatase form up to 500°C. Heating the sample above 550°C, however, causes most of the anatase to transform to rutile [14]. Since the carbonization step of sample *TiP* and *PTi* was performed at 900°C, not unexpectedly, both of our Ti-doped carbon gels contain mainly rutile, the estimated anatase content being <10% (Figure 4c). In sample *PCTi*, the absence of Bragg peaks in Figure 4c implies that the Ti-dopant is non-crystalline.

3.3. Application tests

The photocatalytic activity of the three Ti-containing carbon samples (*TiPC*, *PTiC* and *PCTi*) was tested in the decomposition reaction of the test molecules phenol and methylene blue (MEB). Although the methods used were developed for studying the photocatalytic activity of TiO_2 nanoparticles, it is nevertheless possible to estimate the performance of the Ti-doped carbons. However, the analysis of the results regarding the real catalytic activity was hindered in some cases by the high adsorption capacity of the carbon.

Degussa P25 TiO_2 catalyst degraded all the phenol molecules within ca. 80 minutes (Figure 6a). As expected, prior to the UV irradiation, the Ti-doped carbon aerogels adsorbed about 50% of the phenol from the solution, as is shown by the value of the kinetic curves at t=0. The most effective was *PTiC*, which reduced the phenol concentration in the solution to 25% of the original value during the experiment. With the other two samples, after the immediate adsorption step, the phenol concentration remained constant within experimental error (Figure 6a). The

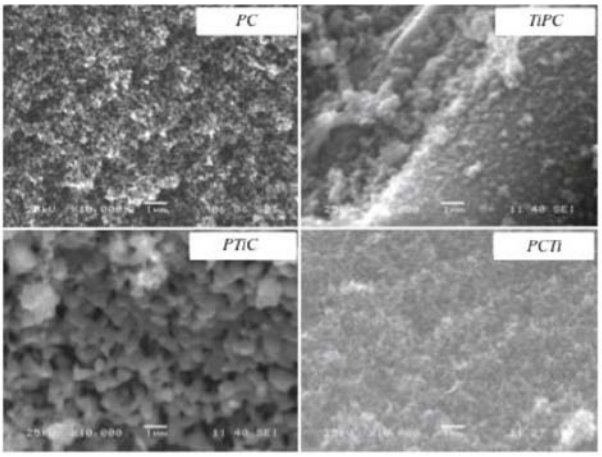

Figure 5. SEM images (x10000, scalebar = 1 μm) of the carbon gels.

Table 3. Data from SAXS curves of PC and the Ti-doped derivates.

Sample	*R* Å
PC	57
TiPC	45
PTiC	20
PCTi	70

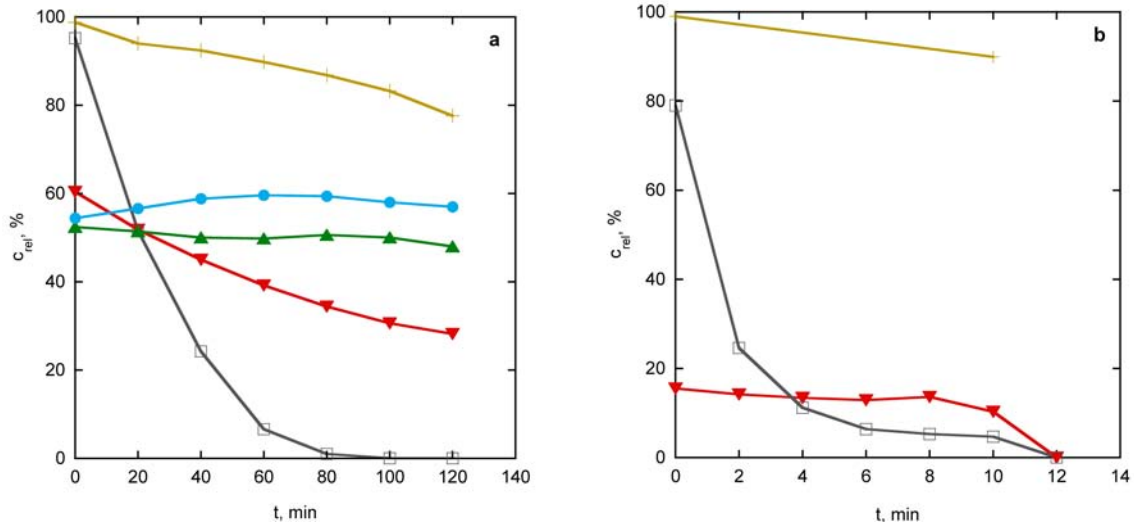

Figure 6. Efficiency of (a) phenol (b) methylene blue removal. No catalyst (+), Degussa P25 TiO_2 (□), TiPC (▲), PTiC (▼) and PCTi (●). $c_{rel}=c/c_0\times100$, where c: measured concentration (M), c_0: initial concentration (M).

values of the BET parameter *C* and the DR slope in Table 2 show that this sample has the most carbon-like surface character, which suggests that in *TiPC* the crystalline TiO_2 is covered by the carbon matrix, thereby inhibiting its catalytic activity, while the catalytic inactivity of *PCTi* is certainly the result of the amorphous character of TiO_2.

Figure 6b compares the decomposition of MEB of *PTiC* sample with that of *Degussa P25 TiO*$_2$ particles (anatase : rutile = 3 : 1). Owing to their high macropore content (which allows easier access to the meso- and micropores) *TiPC* and *PCTi* adsorbed all the test material prior to the irradiation.

While the reduction in MEB concentration by commercial TiO_2 follows a simple exponential decay, the time dependence of sample *PTiC* is more complex. After promptly adsorbing 85% of the MEB this sample behaves as a UV-controlled MEB-source. As MEB degrades, the adsorption equilibrium – through the desorption of MEB – is continuously re-established. Equilibrium between decomposition and desorption resulted in an apparently constant MEB concentration during the first 8 minutes of the experiment. After this delay, degradation becomes dominant. The total decomposition time is the same as that with the pure TiO_2, although the TiO_2 content of the carbon gel is only 72 wt%. Further investigation is needed to explore the application potential of this behavior.

4. Conclusions

The influence of TTIP on the morphology and potential catalytic activity of Ti-containing RF and carbon aerogels have been explored. Addition of the titanium compound in the polymerization stage (*TiP*) prevents the formation of monoliths, and did not yield the typical 3D bead structure of the RF aerogels. The SAXS measurements, however, reveal that the precipitate has a secondary structure consisting of large aggregates. SEM images confirm that the loose structure of the RF aerogel becomes more compact after the doping, which also reduces the N_2 adsorption capacity through pore blocking. The impregnation affects the large-scale structure (i.e., the low *q* regime) of the impregnated samples as well. The radius of the elementary scattering units is ~100 Å in the impregnated aerogels and ~70 Å in the undoped RF gel. Carbonization modifies the structure of the *TiP*, and its surface becomes highly structured, while the other samples conserve their loose morphology. The enhanced microporosity leads to an increase in the N_2 adsorption capacity, while the radius of the scattering units decreases to 20-45 Å. During the heat treatment, the titanium transforms to crystalline TiO_2, which appears as a mixture of anatase and rutile (anatase:rutile≈1:9). The Ti-doped carbon gels exhibited photocatalytic activity by decomposing phenol or methylene blue from aqueous solution. The photocatalytic performance of the *PTiC* sample is comparable to that of the pure TiO_2 (same efficiency in methylene blue decomposition, 70% efficiency in phenol decomposition), although the effective photocatalyst content of our sample is 72%. In addition, owing to the high adsorption capacity, our hybrid catalysts allow an immediate reduction in the amount of the aromatic pollutant in the water. These results suggest that the TiO_2 - carbon aerogel hybrid materials have potential in, e.g., photocatalytic water purification applications.

Acknowledgements

The support of the FP7 Marie Curie IRSES program (project COMPOSITUM, PIRSES-GA-2008-230790) is gratefully acknowledged. This work is related to the scientific program “Development of quality-oriented and harmonized R+D+I strategy and functional model at BME” supported by the New Hungary Development Plan (Project ID: TÁMOP-4.2.1/B-09/1/KMR-2010-0002). Imre M. Szilágyi thanks for a János Bolyai Research Fellowship of the Hungarian Academy of Sciences. We are grateful to the European Synchrotron Radiation Facility for access to the French CRG beam line BM2 and to Cyrille Rochas and György Bosznai for their invaluable assistance. The help of Edit Székely and Imre Dékány is gratefully acknowledged.

References

[1] C. Moreno-Castilla, F.J. Maldonado-Hódar, A.F. Pérez-Cadenas. Physicochemical surface properties of Fe, Co, Ni, and Cu-Doped monolithic organic aerogels. Langmuir, 19, 5650–5655 (2003).

[2] F.J. Maldonado-Hódar, C. Moreno-Castilla, A.F. Pérez-Cadenas. Surface morphology, metal dispersion, and pore texture of transition metal-doped monolithic carbon aerogels and steam-activated derivatives. Microporous Mesoporous Mater., 69, 119–125 (2004).

[3] R. Fu, M.S. Dresselhaus, G. Dresselhaus, B. Zheng, J. Liu, J. Satcher Jr., et al. The growth of carbon nanostructures on cobalt-doped carbon aerogels. J. Non-Cryst. Solids, 318, 223–232 (2003).

[4] F.J. Maldonado-Hódar, M.A. Ferro-García, J. Rivera-Utrilla, C. Moreno-Castilla. Synthesis and textural characteristics of organic aerogels, transition-metal-containing organic aerogels and their carbonized derivatives. Carbon, 37, 1199–1205 (1999).

[5] C. Moreno-Castilla, F.J. Maldonado-Hódar, F. Carraso-Marin, E. Rodriguez-Castellón, Surface characteristics of titania/carbon composite aerogels. Langmuir, 18, 2295–2299 (2002).

[6] M. Sánchez-Polo, J. Rivera-Utrilla, J. Méndez-Díaz, J. López-Peñalver. Metal-doped carbon aerogels. new materials for water treatments. Ind. Eng. Chem. Res., 47, 6001–6005 (2008).

[7] M.L. Rojas-Cervantes, L. Alonso, J. Díaz-Terán, A.J. López-Peinado, R.M. Martín-Aranda, V. Gómez-Serrano. Basic metal–carbons catalysts prepared by sol–gel method. Carbon; 42, 1575–1582 (2004).

[8] N. Fu, R. Yoshizawa, M.S. Dresselhaus, G. Dresselhaus, J.H. Satcher Jr., T.F. Baumann. XPS study of copper-doped carbon aerogels. Langmuir, 18, 10100–10104 (2002).

[9] O. Czakkel, E. Geissler, I.M. Szilágyi, E. Székely, K. László. Cu-doped resorcinol–formaldehyde (RF) polymer and carbon aerogels. J. Colloid Interface Sci., 337, 513–522 (2009).

[10] O. Czakkel, E. Geissler, A. Moussaïd, B. Koczka, K. László. Copper-containing resorcinol–formaldehyde networks. Microporous Mesoporous Mater., 126, 213–221 (2009).

[11] O. Czakkel, B. Nagy, E. Geissler, K. László. Effect of molybdenum on the structure formation of resorcinol-formaldehyde hydrogels studied by coherent X-Ray scattering. J. Chem. Phys., 136, 234907 (2012).

[12] K. Mogyorosi, I. Dékány, J.H. Fendler. Preparation and characterization of clay mineral intercalated titanium dioxide nanoparticles. Langmuir, 19, 2938–2946 (2003).

[13] O. Czakkel, K. Marthi, E. Geissler, K. László. Influence of drying on the morphology of resorcinol–formaldehyde-based carbon gels. Microporous Mesoporous Mater., 86, 124–133 (2005).

[14] F.J. Maldonado-Hódar, C. Moreno-Castilla, J. Rivera-Utrilla. Synthesis, pore texture and surface acid–base character of TiO_2/carbon composite xerogels and aerogels and their carbonized derivatives. Appl. Catal. A, 203, 151–159 (2000)

[15] O. Czakkel, E. Székely, E. Geissler, K. László. Drying of resorcinol–formaldehyde gels with CO_2 medium. Microporous Mesoporous Mater., 148, 34–42 (2012).

[16] S.J. Gregg, K.S.W. Sing, Adsorption, Surface Area and Porosity, Academic Press, London, U.K., 1982.

[17] S. Brunauer, P. Emmett, E. Teller. Adsorption of Gases in Multimolecular Layers. J. Am. Chem. Soc., 60, 309–319 (1938).

[18] J. Ménesi, L. Körösi, E. Bazsó, V. Zöllmer, A. Richardt, I. Dékány. Photocatalytic oxidation of organic pollutants on titania–clay composites. Chemosphere, 70, 538–542 (2008).

[19] N. Balázs, K. Mogyorósi, D.F. Srankó, A. Pallagi, T. Alapi, A. Oszkó, et al. The effect of particle shape on the activity of nanocrystalline TiO2 photocatalysts in phenol decomposition. Appl. Catal. B-Environ., 84, 356–362 (2008).

[20] J. Rouquerol, F. Rouquerol, K. Sing, Adsorption by powders and porous solids, Academic Press, New York, U.S.A., 1999.

[21] W.H. Baur. Atomabstände und Bindungswinkel im Brookit, TiO2. Acta Cryst., 14, 214–216 (1961).

[22] S.D. Mo, W.Y. Ching. Electronic and optical properties of three phases of titanium dioxide: Rutile, anatase, and brookite. Phys. Rev. B, 51, 13023–13032 (1995).

[23] H. Zhang, J.F. Banfield. Thermodynamic analysis of phase stability of nanocrystalline titania. J. Mater. Chem., 8, 2073–2076 (1998).

[24] G. Madrasw, B.J. McCoy, A. Navrotsky. Kinetic model for tio_2 polymorphic transformation from anatase to rutile. J. Am. Ceram. Soc., 90, 250–255 (2007).